Original Paper

Eletrônica de Potência
Open Journal of Power Electronics

Received November 07, 2025; Received in revised form December 16, 2025; Accepted January 19, 2025; Date of publication January 30, 2025.
The review of this paper was arranged by Associate Editor Fabrício Bradaschia and Editor-in-Chief Allan F. Cupertino.
Digital Object Identifier http://doi.org/10.18618/REP.e202610

Analysis and design of a load-independent class-E LCL resonant converter

Lucas S. Mendonça [1,*], Valmir de Oliveira [1], Guilherme S. Simeão [1], Fábio E. Bisogno [2]

[1] Federal University of Technology – Paraná, Academic Department of Electronics, Curitiba, PR, Brazil
[2] Hochschule Koblenz, Lehrgebiet Elektronik, Koblenz, Germany

e-mail: lucasmendonca@utfpr.edu.br* ;valmir@utfpr.edu.br;guilhermesimeao@alunos.utfpr.edu.br;fbisogno@gmail.com.
* Corresponding author.

ABSTRACT This work brings in a load-independent Class-E LCL resonant converter. The intertwined soft-switching and load-independent functions in resonant topologies require high mathematical effort and leads to trade-off designing characteristics related to the operating frequency, output power and load range. Therefore, this paper shows the exact analysis for the Class-E LCL converter by axiomatically dealing with the second, third and fourth-order polynomials. In addition, a design method is proposed based on the implicit equations while considering the soft-switching and load-independence features. The measured built prototype operates at $1.2\,\text{MHz}$, which outperforms most of the state-of-the-art compared converters by $\times 1.2$, while maintaining comparable output power and efficiency ($92\,\%$).

KEYWORDS class-E amplifiers, load-independence, resonant converters

I. INTRODUCTION

Peerless features, like as soft-switching mechanisms and high-frequency/high-efficiency operation, places resonant converters as cutting-edge technologies in alternate current power conversions. Especially in CC/CA inverters, Class-E converters achieve zero-voltage switching (ZVS) and zero-derivative-voltage switching (ZDVS) due to the charge and discharge of the parallel switch capacitance, accomplishing low switching losses and high-efficiency [1]. Modern power electronics enjoy resonant converters in applications like as, wireless power transfer [2]–[5], induction heating [6], [7] and medical [8], [9].

Topologies in resonant power conversion varies in terms of number of switches/reactive elements, switch position, soft-switching mechanism and load characteristic. The most well-known examples are, Class-D [10], [11], Class-E [12], [13] and Class-F converters [14]. In almost all cases, the design complexity arises from the high number of passive elements and the soft-switching conditions, leading to high mathematical effort to find the analytical solutions [15]–[17]. In addition, Class-E converters are sensitive to load variation. However, practical applications require stable output voltage or current [18], [19].

Besides the closed-loop solution, with dynamic dead-time [20], hysteresis control [21], and frequency control [22], [23], recent research demonstrates the feasibility of load-independence Class-E conversion without feedback controllers. In [24], a finite inductor is replaced in the standard Class-E topology to achieve load-independence with $92.7\,\%$ efficiency at $1\,\text{MHz}$. By creating a resonant structure with a switch capacitance and a shunt inductance, [25] has provided a Class-E^{-1} circuit operating with ZVS constant current mode. A similar topology is shown in [26], however, it provides a zero-current switching (ZCS) constant voltage operation. Besides the soft-switching and the type of constant output, it is interesting to evaluate the load range. In [27], a parallel Class-E resonant inverter with floating-ground switch performs improved load operating range ($\times 40$) with conversion efficiency from $37.7 - 89.3\,\%$.

Ubiquitous, there is a trade-off among load range, input current ripple, component size, operating frequency and output power, which leads to increased analysis and design complexity [28]. Furthermore, in order to achieve load-independent operation and keep the soft-switching conditions, it is necessary to find two exact analytical solutions [27], [29], [30]: 1) A function dependent on the normalized resonant frequency and duty cycle times the input voltage; 2) A function dependent on the normalized resonant frequency, duty cycle, and output voltage/current phase times the output amplitude current times the input impedance. By ensuring that both aforementioned functions are zero in the switch transition instant, load-independence is achieved with ZVS/ZCS operation. Notwithstanding, the aforementioned functions require unique equating regarding topological configuration.

In this sense, this paper provides the exact analysis and design methodology of a Class-E LCL converter. The proposed topology has a LCL-network between the main resonant tank and the output load. The topology is interesting in inductive wireless power transfer applications because

the transmitter coil inductance can be used as the output inductor of the LCL tank, reducing hardware size while ensuring the Class-E topology advantages. The analysis is performed by equating the electrical variables based on sine, cosine and exponential terms, so, it is shown how to deal with second, third and fourth-order polynomials generated in the complex frequency domain equating. By providing the exact solution, it is possible to find a governing equation for the switch voltage that reveals the soft-switching-load-independent intertwined functions. In addition, a design methodology is proposed based on implicit equations that are numerically solved in order to find the reactive component values. A 1.2 MHz prototype is experimentally validated to confirm the theoretical approach and evaluate the load-independence range.

II. MATHEMATICAL APPROACH

The proposed Class-E LCL resonant converter is composed of an input voltage V_{in}, input inductor L_c, switch S, inverter capacitor C_p, resonant capacitor C_o, resonant inductor L_o, LCL-network L_{r1}-C_{r1}-L_{r2} and load R as depicted in Fig. 1. In addition, by considering the LCL-network frequency equals to the switching frequency, the Class-E converter drives an equivalent load Z_o.

Axiom 1. *The inductors in the LCL-network are equal:* $L_{r1} = L_{r2}$.

Axiom 2. *The LCL-network angular frequency is equal to the angular switching frequency:* $\omega_{LCL} = \omega$.

Lemma 1. *The LCL-network can be represented by an equivalent load* Z_o *for the Class-E inverter described by* $Z_o = L_{r1}/RC_{r1}$.

Proof:
The LCL-network can be described in the s-domain frequency as:

$$Z_o = (R + sL_{\text{r2}})//\left(\frac{1}{sC_{\text{r1}}}\right) + sL_{\text{r1}}, \tag{1}$$

then

$$Z_o = \frac{s^3 L_{\text{r1}} L_{\text{r1}} C_{\text{r1}} + s^2 R L_{\text{r1}} C_{\text{r1}} + sL_{\text{r1}} + sL_2 + R}{s^2 L_2 C_{\text{r1}} + sRC_{\text{r1}} + 1}, \tag{2}$$

by taking into account Axioms 1 and 2:

$$Z_o = \frac{-sL_{\text{r1}} - R + sL_{\text{r1}} + sL_{\text{r1}} + R}{sRC_{\text{r1}} + 1 - 1} = \frac{L_{\text{r1}}}{RC_{\text{r1}}}. \tag{3}$$

■

A. Exact Time-Domain Solutions

In order to analyze the converter, two operating stages are considered: switch S on/off ruled by duty cycle D_c. In addition, the output current is described as a pure sinusoid waveform.

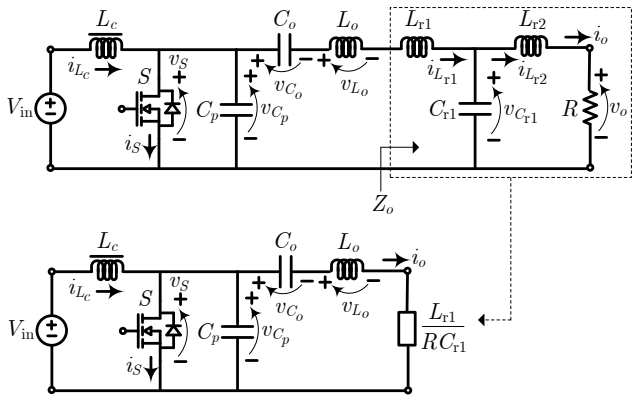

FIGURE 1. Class-E LCL resonant converter.

Axiom 3. *The load quality factor is sufficiently high, therefore, the output current is*

$$i_o(t) = I_o \sin(\omega t + \phi), \tag{4}$$

in which, I_o is the amplitude and ϕ the phase. In this regard, the equivalent circuits to be analyzed are shown in Fig. 2(a) and in Fig. 2(b). I_1 and I_2 are the loop currents, which describe the input inductor current and the output current, respectively.

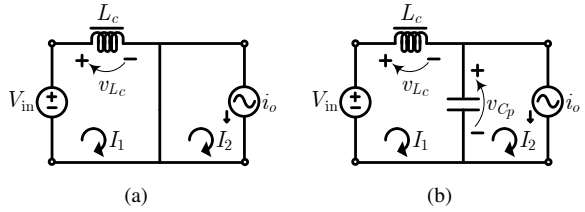

FIGURE 2. Class-E LCL topology. (a) Switch S on. (b) Switch S off.

When switch S is on, the governing equation in first loop is given as

$$-V_{\text{in}} + v_{L_c}(t) = 0, \tag{5}$$

which is described in the s-domain by

$$-\frac{V_{\text{in}}}{s} + sL_c I_1(s) - L_c i_1(0) = 0, \tag{6}$$

therefore,

$$I_1(s) = \frac{V_{\text{in}}}{s^2 L_c} + \frac{i_1(0)}{s}, \tag{7}$$

which can be converted to the time-domain by using the Laplace Inverse Transform by means of the known Laplace pairs:

$$\overset{\text{I}}{i_1}(t) = \left(\frac{V_{\text{in}}}{L_c}\right)t + i_1(0)\,\text{A}. \tag{8}$$

Due to the parallel connection to the switch S, the capacitor C_p voltage is:

$$\overset{\text{I}}{v_{C_p}}(t) = 0\,\text{V}. \tag{9}$$

When switch S is off, the governing equation related to the $V_{\text{in}} - L_c - C_p$ loop is

$$-V_{\text{in}} + v_{L_c}(t) + v_{C_p}(t) = 0, \tag{10}$$

which is rewritten in the complex frequency domain by

$$\frac{-V_{\text{in}}}{s} + sL_cI_1(s) - L_c i_1(D_c 2\pi) + \frac{I_1(s) - I_2(s)}{sC_p} + \frac{v_{C_p}(D_c 2\pi)}{s} = 0, \tag{11}$$

being $i_1(D_c 2\pi)$ and $v_{C_p}(D_c 2\pi)$ the initial conditions and $I_2 = i_o$. Further rearranging leads to:

$$\begin{aligned} I_1(s) = {} & V_{\text{in}}\left(\frac{C_p}{s^2 L_c C_p + 1}\right) + L_c i_1(Dc2\pi)\left(\frac{sC_p}{s^2 L_c C_p + 1}\right) \\ & - v_{C_p}(D_c 2\pi)\left(\frac{C_p}{s^2 L_c C_p + 1}\right) + I_o\left(\frac{s\sin(\phi) + \omega\cos(\phi)}{s^2 + \omega^2}\right) \\ & \times \left(\frac{1}{s^2 L_c C_p + 1}\right). \end{aligned} \tag{12}$$

Mathematical operations should be conducted to adequate the equation into the well-known Laplace pairs. Second-order polynomials are modified by the completing the square method. On the other hand, fourth-order polynomials need the expansion in partial fractions.

Axiom 3. *Second-order polynomials can be rewritten as:*

$$\frac{1}{a_1 s^2 + b_1 s + c_1} = \frac{1}{a_1\left[(s + \alpha_1)^2 + \beta_1\right]} \tag{13}$$

in which, $\alpha_1 = b_1/2a_1$ and $\beta_1 = c_1/a_1 - \alpha_1^2$.

Axiom 4. *Third and fourth-order polynomials are rewritten as:*

$$\left(\frac{s\sin(\phi) + \omega\cos(\phi)}{s^2 + \omega^2}\right)\left(\frac{1}{a_1 s^2 + c_1}\right) = \frac{A_1 s + B_1}{s^2 + \omega_2} + \frac{C_1 s + D_1}{a_1 s + c_1}, \tag{14}$$

with constants: $A_1 = -\frac{\sin(\phi)}{-c_1 + a_1\omega^2}$, $B_1 = -\frac{\omega\cos(\phi)}{-c_1 + a_1\omega^2}$, $C_1 = \frac{a_1\sin(phi)}{-1 + a_1\omega_2}$ and $D_1 = \frac{a_1\omega\cos(\phi)}{-1 + a_1\omega^2}$.

Therefore, Equation (12) is expressed as

$$\begin{aligned} I_1(s) = {} & \frac{V_{\text{in}}C_p}{a_1\sqrt{\beta_1}}\left[\frac{\sqrt{\beta_1}}{(s + \alpha_1)^2 + \beta_1}\right] + \frac{L_c C_p i_1(D_c 2\pi)}{a_1} \\ & \times \left[\frac{s + \alpha_1}{(s + \alpha_1)^2 + \beta_1}\right] - \frac{L_c C_p i_1(D_c 2\pi)\alpha_1}{a_1\sqrt{\beta_1}} \\ & \times \left[\frac{\sqrt{\beta_1}}{(s + \alpha_1)^2 + \beta_1}\right] - \frac{C_p v_{C_p}(D_c 2\pi)}{a_1\sqrt{\beta_1}} \\ & \times \left[\frac{\sqrt{\beta_1}}{(s + \alpha_1)^2 + \beta_1}\right] + I_o\left[A_1\left(\frac{s}{s^2 + \omega^2}\right)\right. \\ & + \frac{B_1}{\omega}\left(\frac{\omega}{s^2 + \omega^2}\right) + \frac{C_1}{L_c C_p}\left(\frac{s}{s^2 + \frac{1}{L_c C_p}}\right) \\ & \left. + \frac{D_1}{L_c C_p}\left(\frac{1}{s^2 + \frac{1}{L_c C_p}}\right)\right], \end{aligned} \tag{15}$$

with $a_1 = L_c C_p$, $b_1 = 0$ and $c_1 = 1$. By applying the inverse Laplace Transform, the time-domain solution is obtained as:

$$\begin{aligned} i_1^{\text{II}}(t) = {} & \frac{V_{\text{in}}C_p}{a_1\sqrt{\beta_1}}\left[e^{-\alpha_1 t}\sin\left(\sqrt{\beta_1}t\right)\right] + \frac{L_c C_p i_1(D_c 2\pi)}{a_1} \\ & \times \left[e^{-\alpha_1 t}\cos\left(\sqrt{\beta_1}t\right)\right] - \frac{L_c C_p i_1(D_c 2\pi)\alpha_1}{a_1\sqrt{\beta_1}} \\ & \times \left[e^{-\alpha_1 t}\sin\left(\sqrt{\beta_1}t\right)\right] - \frac{C_p v_{C_p}(D_c 2\pi)}{a_1\sqrt{\beta_1}} \\ & \times \left[e^{-\alpha_1 t}\sin\left(\sqrt{\beta_1}t\right)\right] + I_o\left[A_1\cos(\omega t)\right. \\ & + \frac{B_1}{\omega}\sin(\omega t) + \frac{C_1}{L_c C_p}\cos\left(\sqrt{\frac{1}{L_c C_p}}t\right) \\ & \left. + \frac{D_1}{L_c C_p}\sin\left(\sqrt{\frac{1}{L_c C_p}}t\right)\right] \text{A}. \end{aligned} \tag{16}$$

Equating for $v_{C_p}(t)$ in the complex frequency domain leads to:

$$V_{C_p}(s) = \frac{1}{sC_p}I_1(s) - \frac{1}{sC_p}(s)I_2(s) + \frac{1}{s}v_{C_p}(D_c T), \tag{17}$$

which is re-written considering (12) as

$$\begin{aligned} V_{C_p}(s) = {} & \frac{V_{\text{in}}}{s}\left(\frac{1}{s^2 L_c C_p + 1}\right) + L_c i_1(Dc2\pi)\left(\frac{1}{s^2 L_c C_p + 1}\right) \\ & - \frac{v_{C_p}(D_c 2\pi)}{s}\left(\frac{1}{s^2 L_c C_p + 1}\right) + \frac{I_o}{C_p}\frac{1}{s} \\ & \times \left(\frac{s\sin(\phi) + \omega\cos(\phi)}{s^2 + \omega^2}\right)\left(\frac{1}{s^2 L_c C_p + 1}\right) \\ & - \frac{I_o}{C_p}\frac{1}{s}\left(\frac{s\sin(\phi) + \omega\cos(\phi)}{s^2 + \omega^2}\right) + \frac{1}{s}v_{C_p}(D_c T). \end{aligned} \tag{18}$$

By taking advantage of Axioms 4 and 5, the following is achieved:

$$\begin{aligned} V_{C_p}(s) = {} & \frac{E_1}{L_c C_p}\left(\frac{s}{s^2 + \frac{1}{L_c C_p}}\right) + \frac{F_1\sqrt{L_c C_p}}{L_c C_p}\left(\frac{\sqrt{1/L_c C_p}}{s^2 + \frac{1}{L_c C_p}}\right) \\ & + \frac{G_1}{s} + \frac{i_1(D_c T)\sqrt{C_p}}{L_c C_p}\left(\frac{\sqrt{1/L_c C_p}}{s^2 + \frac{1}{L_c C_p}}\right) - \frac{L_1}{L_c C_p} \\ & \times \left(\frac{s}{s^2 + \frac{1}{L_c C_p}}\right) - \frac{M_1\sqrt{L_c C_p}}{L_c C_p}\left(\frac{\sqrt{1/L_c C_p}}{s^2 + \frac{1}{L_c C_p}}\right) \\ & - \frac{N_1}{s} + O_1\left(\frac{s}{s^2 + \omega^2}\right) + \frac{P_1}{\omega}\left(\frac{\omega}{s^2 + \omega^2}\right) \\ & \frac{Q_1}{L_c C_p}\left(\frac{s}{s^2 + \frac{1}{L_c C_p}}\right) + \frac{R_1\sqrt{L_c C_p}}{L_c C_p}\left(\frac{\sqrt{1/L_c C_p}}{s^2 + \frac{1}{L_c C_p}}\right) \\ & + \frac{S_1}{s} - T_1\left(\frac{s}{s^2 + \omega^2}\right) - \frac{U_1}{\omega}\left(\frac{\omega}{s^2 + \omega^2}\right) \\ & - \frac{V_1}{s} + \frac{v_{C_p}(D_c T)}{s}, \end{aligned} \tag{19}$$

with constants: $E_1 = -C_pL_cV_{\text{in}}$, $F_1 = 0$, $G_1 = V_{\text{in}}$, $H_1 = -C_pL_c^2 i_1(D_c 2\pi)$, $J_1 = 0$, $K_1 = L_c i_1(D_c 2\pi)$, $L_c = -C_pL_c v_{C_p}(D_c 2\pi)$, $M_1 = 0$, $N_1 = v_{C_p}(D_c 2\pi)$, $O_1 = \frac{I_o\cos(\phi)}{C_p\omega(-1+C_pL_c\omega^2)}$, $P_1 = -\frac{I_o\sin(\phi)}{C_p(-1+C_pL_c\omega^2)}$, $Q_1 = -\frac{C_pI_oL_c^2\omega\cos(\phi)}{-1+C_pL_c\omega^2}$, $R_1 = \frac{I_oL_c\sin(\phi)}{-1+C_pL_c\omega^2}$, $S_1 = \frac{I_o\cos(\phi)}{C_p\omega}$, $T_1 = -\frac{I_o\cos(\phi)}{C_p\omega}$, $U_1 = \frac{I_o\sin(\phi)}{C_p}$ and $V_1 = \frac{I_o\cos(\phi)}{C_p\omega}$. Therefore, the time-domain solution is written by

$$
\begin{aligned}
v_{C_p}^{\text{II}}(t) = &\frac{E_1}{L_cC_p}\cos\left(\sqrt{\frac{1}{L_cC_p}}t\right) + \frac{F_1\sqrt{L_cC_p}}{L_cC_p}\sin\left(\sqrt{\frac{1}{L_cC_p}}t\right) \\
&+ G_1 + \frac{i_1(D_cT)\sqrt{L_cC_p}}{C_p}\sin\left(\sqrt{\frac{1}{L_cC_p}}t\right) - \frac{L_1}{L_cC_p} \\
&\times\cos\left(\sqrt{\frac{1}{L_cC_p}}t\right) - \frac{M_1\sqrt{L_cC_p}}{L_cC_p}\sin\left(\sqrt{\frac{1}{L_cC_p}}t\right) \\
&- N_1 + O_1\cos(\omega t) + \frac{P_1}{\omega}\sin(\omega t) \\
&\frac{Q_1}{L_cC_p}\cos\left(\sqrt{\frac{1}{L_cC_p}}t\right) + \frac{R_1\sqrt{L_cC_p}}{L_cC_p}\sin\left(\sqrt{\frac{1}{L_cC_p}}t\right) \\
&+ S_1 - T_1\cos(\omega t) - \frac{U_1}{\omega}\sin(\omega t) - V_1 + v_{C_p}(D_cT)\,\text{V}.
\end{aligned}
\tag{20}
$$

B. Load-Independent Conditions

In order to find the load-independent operating point, the switch voltage v_S governing equation is considered as

$$
v_S(\omega t) = \Psi_1(q, D_c)\times V_{\text{in}} + \Psi_2(q, D_c, \phi)\times I_oZ_{\text{in}}, \tag{21}
$$

in which, Ψ_1 is a function dependent on D_c and the normalized resonant frequency $q = 1/\omega\sqrt{L_cC_p}$ and Ψ_2 is a function dependent on I_o and the input impedance $Z_{\text{in}} = \sqrt{L_c/C_p}$, described in detail as ($\bar{D}_c = 1 - D_c$):

$$
\begin{aligned}
\Psi_1(q, D_c) = &\left[\frac{1}{q^2} - \frac{1}{q^4} - \frac{2\cos(q2\pi\bar{D}_c)}{q^2} + \frac{2\cos(q2\pi\bar{D}_c)}{q^4}\right. \\
&+\frac{\cos(q2\pi\bar{D}_c)^2}{q^2} - \frac{\cos(q2\pi\bar{D}_c)^2}{q^4} + \frac{2\pi D_c\sin(q2\pi\bar{D}c)}{q} \\
&\left.-\frac{2\pi D_c\sin(q2\pi\bar{D}c)}{q^3} + \frac{\sin(q2\pi\bar{D}_c)^2}{q^2} - \frac{\sin(q2\pi\bar{D}_c)^2}{q^4}\right] \\
&\Big/\left[\left(\frac{-1}{q^2} + \frac{1}{q^4}\right)\Big(-1 + \cos(q2\pi\bar{D}_c)\Big)\right]
\end{aligned}
\tag{22}
$$

and

$$
\begin{aligned}
\Psi_2(q, D_c, \phi) = &\left[\frac{\cos(q2\pi\bar{D}_c)\cos(\phi)}{q^3} - \frac{\cos(q2\pi\bar{D}_c)^2\cos(\phi)}{q^3}\right. \\
&-\frac{\cos(2\pi\bar{D}_c)\cos(\phi)}{q^3} + \frac{\cos(q2\pi\bar{D}_c)\cos(2\pi\bar{D}_c+\phi)}{q^3} \\
&-\frac{\sin(q2\pi\bar{D}_c)^2\cos(\phi)}{q^3} - \frac{\sin(q2\pi\bar{D}_c)\sin(\phi)}{q^2} \\
&+\frac{\cos(2\pi\bar{D}_c)\sin(q2\pi\bar{D}_c)\sin(\phi)}{q^2} \\
&+\frac{\sin(2\pi\bar{D}_c)\sin(q2\pi\bar{D}_c)\cos(\phi)}{q^2} \\
&\left.+\frac{\sin(2\pi\bar{D}_c)\sin(\phi)}{q^3}\right] \\
&\Big/\left[\left(\frac{-1}{q^2} + \frac{1}{q^4}\right)\Big(-1 + \cos(q2\pi\bar{D}_c)\Big)\right].
\end{aligned}
\tag{23}
$$

Lemma 2. *The load-independent operation is achieved by satisfying $\Psi_1(q, D_c) = 0$ and $\Psi_2(q, D_c, \phi) = 0$.*

Proof:
Considering $\omega t = 0$, the switch S voltage is zero, under ZVS operation. In order to satisfy $v_S = 0$ for any load while ensuring power transfer, $V_{\text{in}} \neq 0$ and $I_{\text{o}}Z_{\text{in}} \neq 0$. Therefore, $\Psi_1(q, D_c) = 0$ and $\Psi_2(q, D_c, \phi) = 0$. ■

Taking $\Psi_1(q, D_c) = 0$ and $\Psi_2(q, D_c, \phi) = 0$ and applying a parametric sweep into D_c in (22), q can be numerically found for any operating point. Subsequently, (23) is solved in order to find ϕ. Therefore, the load-independent operation requires specific values for q and ϕ dependent on the duty cycle. The normalized resonant frequency q as function of D_c and phase ϕ as function of D_c are depicted in Fig. 3. It can be seen that, load independence is only achieved if $q > 1$.

Aiming to relate the minimum load $R_{o_{\text{min}}}$ to the input impedance Z_{in}, the ZDVS condition is considered: $i_{C_p}^{\text{II}}(T) =$

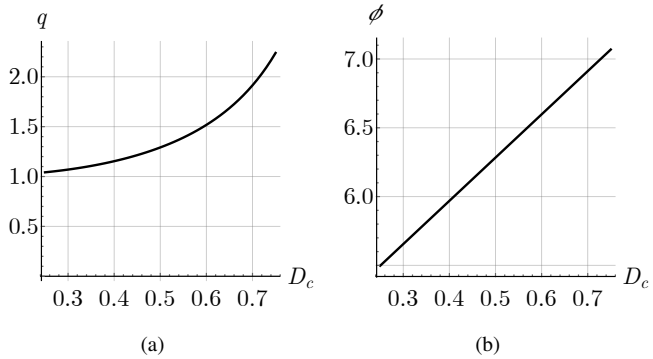

FIGURE 3. Load-independent conditions. (a) q as function of D_c. (b) ϕ as function of D_c.

0, which is written as

$$\Psi_3(L_c, C_p, \omega, \phi, D_c, T)\times I_o+\Psi_4(L_c, C_p, \omega, D_c, T)\times\frac{V_{\text{in}}}{Z_{\text{in}}}=0, \tag{24}$$

being:

$$\begin{aligned}\Psi_3 = &\left[C_p\left(\frac{1}{C_pL_c}\right)^{3/2}\left[2C_pL_c^2\omega\cos(\phi)\right.\right.\\
&\times\sin\left((-1+D_c)\sqrt{\frac{1}{C_pL_c}}T\right)-2L_c\sqrt{C_pL_c}\\
&\times\cos\left(\sqrt{\frac{1}{C_pL_c}}(T-D_cT)\right)\sin(\phi)\\
&+2C_p^2\sqrt{\frac{1}{C_pL_c}}L_c^3\omega^2\sin(\phi-(-1+D_c)T\omega)\\
&+2L_c\sqrt{C_pL_c}\cos\left(\sqrt{\frac{1}{C_pL_c}}(T-D_cT)\right)\\
&\times\sin(\phi+T\omega-D_cT\omega)-2C_p^2\sqrt{\frac{1}{C_pL_c}}L_c^3\omega^2\\
&\left.\left.\times\cos\left(\sqrt{\frac{1}{C_pL_c}}(T-D_cT)\right)\sin(\phi+T\omega-D_cT\omega)\right]\right.\\
&\left./2\left(-1+C_pL_c\omega^2\right)\left(-1+\cos\left(\sqrt{\frac{1}{C_pL_c}}(T-D_cT)\right)\right)\right]\end{aligned} \tag{25}$$

and

$$\begin{aligned}\Psi_4 = &\left[\frac{1}{C_pL_c}\left[2D_c\sqrt{C_pL_c}T\cos\left(\sqrt{\frac{1}{C_pL_c}}(T-D_cT)\right)\right.\right.\\
&-2C_pD_cL_c\sqrt{C_pL_c}T\omega^2\cos\left(\sqrt{\frac{1}{C_pL_c}}(T-D_cT)\right)\\
&-2C_pL_c\sin\left((-1+D_c)\sqrt{\frac{1}{C_pL_c}}T\right)+2C_p^2L_c^2\omega^2\\
&\times\sin\left((-1+D_c)\sqrt{\frac{1}{C_pL_c}}T\right)+C_pL_c\\
&\times\sin\left(2(-1+D_c)\sqrt{\frac{1}{C_pL_c}}T\right)-C_pL_c\\
&\times\sin\left(2(-1+D_c)\sqrt{\frac{1}{C_pL_c}}T\right)-C_p^2L_c^2\omega^2\\
&\times\sin\left(2(-1+D_c)\sqrt{\frac{1}{C_pL_c}}T\right)\\
&\left.\left./2\left(-1+C_pL_c\omega^2\right)\left(-1+\cos\left(\sqrt{\frac{1}{C_pL_c}}(T-D_cT)\right)\right)\right]\right..\end{aligned} \tag{26}$$

III. DESIGN METHODOLOGY

In order to design the converter, the exact time-domain solutions and the load-independent conditions are evaluated in an iterative method that calculates the reactive element values, component stress and load range for any operating point. The time-domain equations are dependent on 11 variables: V_{in}, ω, I_{o}, D_c, L_c, C_p, ϕ, $i_1(0)$, $i_1(D_cT)$, $v_{C_p}(0)$ and $v_{C_p}(D_cT)$. Thus, V_{in}, $\omega = 2\pi f$ and I_{o} are specifications, with f as the operating frequency. In addition, $v_{C_p}(0) = v_{C_p}(D_cT) = 0$ is the ZVS condition. By parameter sweeping D_c, calculate q and ϕ based on the load-independent conditions and using the exact time-domain solutions as a linear system:

$$\begin{pmatrix} \overset{\text{II}}{i_1}(T) \\ \overset{\text{II}}{v_{C_p}}(T) \\ \overset{\text{I}}{i_{L_1}}(D_cT) \\ \left.\frac{d\overset{\text{II}}{i_1}(t)}{dt}\right|_{t=T} \end{pmatrix} - \begin{pmatrix} i_1(0) \\ v_{C_p}(0) \\ i_1(D_cT) \\ \frac{V_{\text{in}}}{L_c} \end{pmatrix} = \begin{pmatrix} 0 \\ 0 \\ 0 \\ 0 \end{pmatrix}, \tag{27}$$

the remaining variables, L_c, C_p, $i_1(0)$ and $i_1(D_cT)$ are found for any operating point. The output load is calculated as $R = V_o/I_o$, where the amplitude output voltage V_o is

$$V_o = \frac{2}{T}\int_{D_cT}^{T} \overset{\text{II}}{v_{C_p}}(t)\sin(\omega t+\phi)dt, \tag{28}$$

and the minimum and maximum output load are

$$R_{o_{\text{min}}} = -\frac{\Psi_3}{\Psi_4}\frac{V_o}{V_{\text{in}}}Z_{\text{in}} \tag{29}$$

and

$$R_{o_{\text{max}}} = \frac{L_{\text{r1}}}{C_{\text{r1}}}\frac{1}{R_{o_{\text{min}}}}, \tag{30}$$

with LCL circuit designed as

$$L_{\text{r1}} = L_{\text{r2}} = \frac{V_o}{I_o\omega} \tag{31}$$

and

$$C_{\text{r1}} = \frac{1}{\omega^2 L_{\text{r1}}}. \tag{32}$$

Finally, with quality factor Q_{L}, the main resonant circuit is found as follows:

$$L_o = \frac{Q_{\text{L}}R_{o_{\text{min}}}}{\omega} \tag{33}$$

and

$$C_o = \frac{1}{\omega^2 L_o}. \tag{34}$$

The design specifications are shown in Table 1. The approximations for the initial conditions and reactive elements, required to numerically solve (27), are detailed in Table 2. The obtained theoretical waveforms for different duty cycles are depicted in Fig. 4. The switch stresses are drawn in Fig. 5. If $D_c > 0.5$, higher is both the peak switch current $I_{S_{\text{peak}}}$ and peak switch voltage $V_{S_{\text{peak}}}$. At lower D_c values, $I_{S_{\text{peak}}}$ is reduced, however, $V_{S_{\text{peak}}}$ increases. The designed L_c and C_p as function of D_c are highlighted in Fig. 6. The described results are used to design the converter aiming the experimental validation.

TABLE 1. Design Specifications.

Parameter	Value
Input DC voltage, V_{in}	11 V
Operating frequency, f_s	1.2 MHz
Output current, I_o	1.3 A
Duty cycle, D_c	$0.2 - 0.8$

TABLE 2. Approximations to Numerically Solve the Linear System.

Quantity	Value
Initial input current, $i_1(0)$	2.00913 A
On-off transition input current, $i_1(D_cT)$	3.03560 A
Inductance, L_{co}	1.78605 μH
Capacitance, C_{po}	9.41566 nF

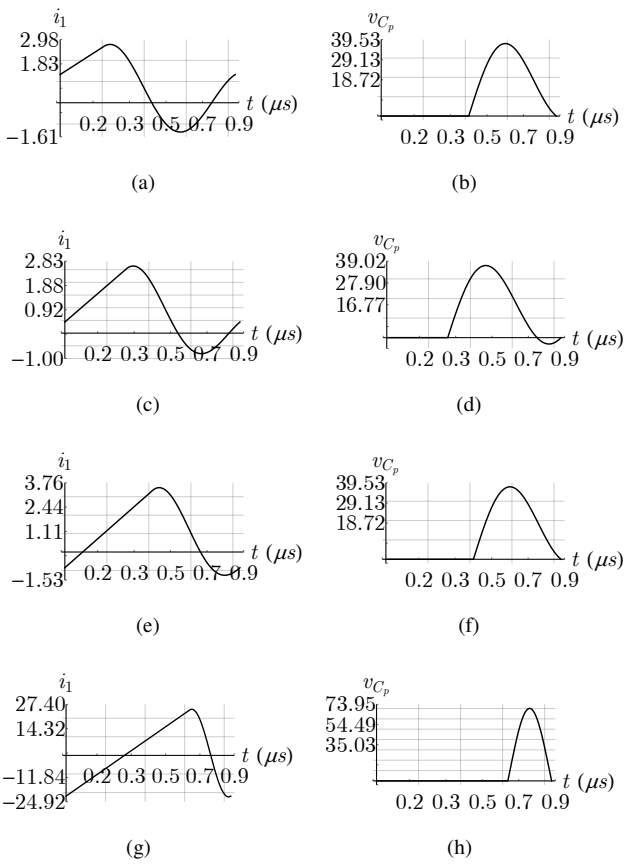

FIGURE 4. Theoretical waveforms for different duty cycles. (a) i_1 **for** $D_c = 0.25$**. (b)** v_{C_p} **for** $D_c = 0.25$**. (c)** i_1 **for** $D_c = 0.35$**. (d)** v_{C_p} **for** $D_c = 0.35$**. (e)** i_1 **for** $D_c = 0.50$**. (f)** v_{C_p} **for** $D_c = 0.50$**. (g)** i_1 **for** $D_c = 0.75$**. (h)** v_{C_p} **for** $D_c = 0.75$**.**

IV. EXPERIMENTAL RESULTS

By considering $D_c = 0.5$, the specifications and components for the designed converter are detailed in Table 3. The IRF510 MOSFET was used as main switch activated by the IRS2011PBF gate-driver. Results were obtained by a Tektronix MSO2024 Oscilloscope with a TCP0020 current probe (1:2 attenuation). Component inductance and capacitance were measured by means of a R&S HM8118 LCR Bridge.

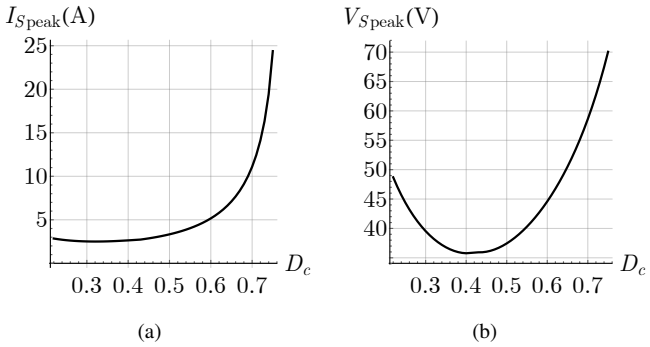

FIGURE 5. Switch stresses. (a) $I_{S_{\text{peak}}}$ **as function of** D_c**. (b)** $V_{S_{\text{peak}}}$ **as function of** D_c**.**

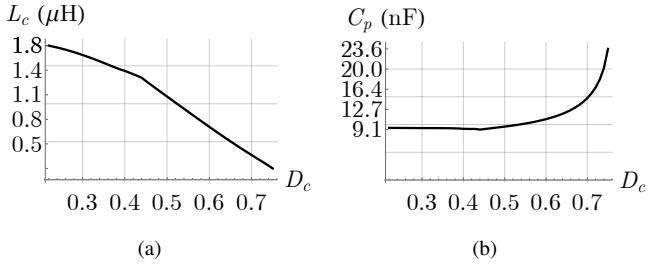

FIGURE 6. Component values. (a) L_c **as function of** D_c**. (b)** C_p **as function of** D_c**.**

The experimental results are shown in Fig. 7 for gate signal voltage v_{G}, switch voltage v_S, output voltage v_o and input inductor current i_{L_c}, considering different loads. ZVS is maintained in all cases with small or negligible delay in contrast to the off-on gate signal transition. In order to evaluate the load-independence, the load was varied from $2.2\,\Omega$ to $25\,\Omega$, and the amplitude output current I_o was measured. Fig. 8 compares the measured I_o to the setpoint 1.3 A and the theoretical constant current (CC) range, which confirms the designed span from 7.9 to $14.7\,\Omega$ ($10\,\Omega$ nominal), ensuring load-independence. Fig. 9 shows the efficiency as function of output power. The calculated power density is $3.16\,\text{W}/\text{mm}^3$. A comparison to related works is detailed in Table 4. With the exception of [26], all compared works use finite input inductor, which leads to reduced inductance value.

TABLE 3. Designed Converter.

Component	Value	Specification
Input inductor, L_c	1.09 μH	Handcrafted (AWG 19)
Parallel capacitor, C_p	10 nF	Ceramic disc
Resonant inductor, L_o	3.16 μH	Handcrafted (AWG 19)
Resonant capacitor, C_o	5.6 nF	Ceramic disc
LCL input inductor, L_{r1}	1.78 μH	Handcrafted (AWG 19)
LCL output inductor, L_{r2}	1.78 μH	Handcrafted (AWG 19)
LCL capacitor, C_{r1}	10 nF	Ceramic disc

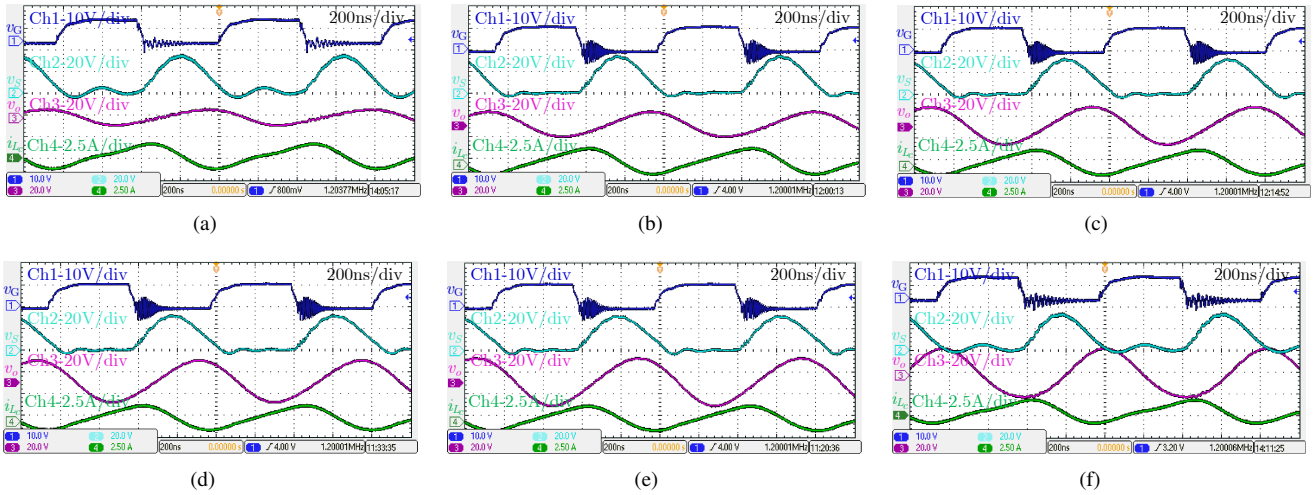

FIGURE 7. Experimental results for gate signal voltage v_G, switch voltage v_S, output voltage v_o and input inductor current i_{L_c}. (a) $R = 3.2\,\Omega$. (b) $R = 10\,\Omega$. (c) $R = 12.9\,\Omega$. (d) $R = 14.2\,\Omega$. (e) $R = 15\,\Omega$. (f) $R = 25\,\Omega$.

TABLE 4. Comparison to Related Works.

Work	Topology	Input inductor	Switching	Output mode	Reactive elements	Power	Load range	Efficiency	Frequency
[24]	Class-E	Finite	ZVS	CC	4	5.85 W	$20-40\,\Omega$	89.3 %	1 MHz
[25]	Class-E^{-1}	Finite	ZVS	CC	6	10.8 W	$1-10\,\Omega$	92.1 %	1 MHz
[26]	Class-E^{-1}	Infinite	ZCS	CV	5	6.96 W	$5-100\,\Omega$	94.4 %	1 MHz
[27]	Floating-gnd Class-E	Finite	ZVS	CC	4	6.72 W	$5-20\,\Omega$	89.3 %	1 MHz
[31]	Class-E	Finite	ZVS	CV	4	3.64 W	$30-50\,\Omega$	93.17 %	1 MHz
[32]	Isolated Class-E	Finite	ZVS	CC	5	12 W	$1-30\,\Omega$	87 %	6.78 MHz
This work	Class-E LCL	Finite	ZVS	CC	6	7.2 W	$7.9-14.7\,\Omega$	92 %	1.2 MHz

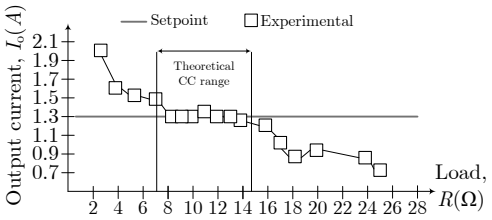

FIGURE 8. Load-independence characteristic.

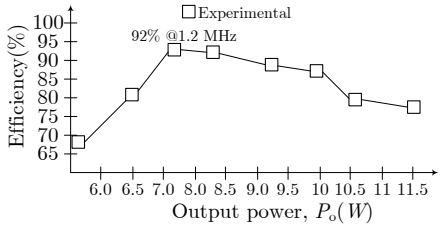

FIGURE 9. Efficiency as function of output power.

Due to the LCL-network, the proposed work has 6 reactive elements, being a drawback in contrast to the standard Class-E topology (4 elements) [24], [31]. The proposed work surpasses by $\times 1.2$ operating frequency all compared works, with exception of [32], which has the lower efficiency. The implemented converter is depicted in Fig. 10. Four loop mitigation barriers were added into the PCB layout to avoid parasitic inductance.

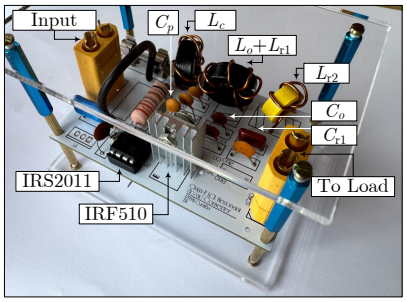

FIGURE 10. Implemented converter.

V. CONCLUSION

A Class-E LCL has been proposed, analyzed, designed and experimentally verified. Due to the high number of components, it was shown how to deal with the high-order polynomials in order to find explicit exact solutions for the electrical variables. The load-independent condition was described based on the normalized resonant frequency, duty cycle and output phase. The converter was designed by a parametric sweep into equations that include the soft-switching conditions. The designed converter outper-

forms most of the compared converters by $\times 1.2$ operating frequency and shows commensurate efficiency. The load-independence was ensured from 7.9 to $14.7\,\Omega$ while keeping ZVS.

AUTHOR'S CONTRIBUTIONS

L.S.MENDONÇA: Conceptualization, Data Curation, Formal Analysis, Methodology, Software, Validation, Writing – Original Draft. **V.OLIVEIRA:** Conceptualization, Data Curation, Funding Acquisition, Investigation, Resources, Validation, Writing – Review & Editing. **G.S.SIMEÃO:** Data Curation, Validation. **F.E.BISOGNO:** Conceptualization, Methodology, Software.

PLAGIARISM POLICY

This article was submitted to the similarity system provided by Crossref and powered by iThenticate – Similarity Check.

DATA AVAILABILITY

The data used in this research is available in the body of the document.

References

[1] M. K. Kazimierczuk, D. Czarkowski, *Resonant Power Converters*, 2 ed., Wiley, 2012.

[2] J.-Q. Zhu, Y.-L. Ban, Y. Zhang, Z. Yan, R.-M. Xu, C. C. Mi, "Three-Coil Wireless Charging System for Metal-Cover Smartphone Applications", *IEEE Transactions on Power Electronics*, vol. 35, no. 5, pp. 4847–4858, 2020, doi:10.1109/TPEL.2019.2944845.

[3] J. Wu, D. Lan, X. Yu, Y. Zheng, R. Xie, Y. Zhang, "An Inductive and Capacitive Hybrid Wireless Power Transfer System for Consumer Electronics with Shared Components", *in 2024 3rd International Conference on Smart Grids and Energy Systems (SGES)*, pp. 86–89, 2024, doi:10.1109/SGES63808.2024.10824149.

[4] F. T. Carneiro, I. Barbi, "A nálise, Projeto e Implementação de um Conversor com Transferência de Energia Sem Fio para Carregadores de Baterias de Veículos Elétricos", *Eletrônica de Potência*, vol. 26, no. 3, pp. 260–267, September 2021, doi:10.18618/REP.2021.3.0003.

[5] R. B. Godoy, E. T. Maddalena, G. de F. Lima, L. F. F. abd V. L. V. Torres, J. O. P. Pinto, "Wireless Charging System With a Non-conventional Compensation Topology for Electric Vehicles and Other Applications", *Eletrônica de Potência*, vol. 21, no. 1, pp. 42–51, March 2016, doi:10.18618/REP.2016.1.2575.

[6] R. A. Hollett, C. H. Lin, D. R. Jensen, J. A. Fan, J. Rivas-Davila, "Design of a Load Invariant Class-E Amplifier for an Inductively Heated Fluidized Bed", *in 2025 IEEE 26th Workshop on Control and Modeling for Power Electronics (COMPEL)*, pp. 1–6, 2025, doi:10.1109/COMPEL57166.2025.11121220.

[7] D. S. Yeole, A. J. Anil, C. P. Pandit, G. V. Vinayak, "Analysis of Compensation Network in Resonant Inductive Power Transfer (RIPT) for Electric Vehicle Charging", *in 2025 5th International Conference on Trends in Material Science and Inventive Materials (ICTMIM)*, pp. 134–137, 2025, doi:10.1109/ICTMIM65579.2025.10988014.

[8] H. Huang, X. Liu, Z. Tang, W. Song, Y. Ma, Y. Zhang, X. Ma, M. Zhang, J. Wang, K. Lu, Z. Wang, G. Li, "A 0.48mm2 Sub-2.4GHz Transceiver with Reused Matching Network and Duty-Cycle Controlled Class-E PA for Medical Band", *in 2024 IEEE Radio Frequency Integrated Circuits Symposium (RFIC)*, pp. 271–274, 2024, doi:10.1109/RFIC61187.2024.10599929.

[9] U. Anwar, K. K. Afridi, D. Markovic, "High-Frequency Resonant Inverter for Power Transfer Between Distributed Modules of a Biomedical Implant", *in 2019 IEEE Energy Conversion Congress and Exposition (ECCE)*, pp. 2426–2431, 2019, doi:10.1109/ECCE.2019.8912952.

[10] S.-A. El-Hamamsy, "Design of high-efficiency RF Class-D power amplifier", *IEEE Transactions on Power Electronics*, vol. 9, no. 3, pp. 297–308, 1994, doi:10.1109/63.311263.

[11] X. Wei, H. Sekiya, T. Nagashima, M. K. Kazimierczuk, T. Suetsugu, "Steady-State Analysis and Design of Class-D ZVS Inverter at Any Duty Ratio", *IEEE Transactions on Power Electronics*, vol. 31, no. 1, pp. 394–405, 2016, doi:10.1109/TPEL.2015.2400463.

[12] W. Zhu, A. Komanaka, Y. Komiyama, H. Koizumi, H. Sekiya, "Simultaneous Wireless Power and Data Transfer System With Reconfigurable Load-Independent Class-E Inverter", *IEEE Journal of Emerging and Selected Topics in Power Electronics*, vol. 13, no. 2, pp. 2622–2632, 2025, doi:10.1109/JESTPE.2024.3508093.

[13] Z. Shu, Y. Fengfa, W. Yijie, J. M. Alonso, "A 500-kHz ZVS Class-E Type DC–DC Converter With Two Anti-Series mosfets Topology", *IEEE Transactions on Power Electronics*, vol. 38, no. 9, pp. 10810–10820, September 2020, doi:10.1109/TPEL.2023.3287161.

[14] S. Aldhaher, D. C. Yates, P. D. Mitcheson, "Load-Independent Class E/EF Inverters and Rectifiers for MHz-Switching Applications", *IEEE Transactions on Power Electronics*, vol. 33, no. 10, pp. 8270–8287, 2018, doi:10.1109/TPEL.2018.2813760.

[15] M. Acar, A. Annema, B. Nauta, "Analytical Design Equations for Class-E Power Amplifiers", *IEEE transactions on circuits and systems I: regular papers*, vol. 54, no. 12, pp. 2706–2717, Dec. 2007, doi:10.1109/TCSI.2007.910544.

[16] P. Kr Gogoi, Ştefănescu, A. Sharma, "Comments on "Analytical Design Equations for Class-E Power Amplifier"", *IEEE Transactions on Circuits and Systems I: Regular Papers*, vol. 72, no. 9, pp. 5297–5298, 2025, doi:10.1109/TCSI.2025.3532202.

[17] B. C. Nicoletti, F. E. Bisogno, L. S. Mendonça, "Exact Solution of the Class-E Inverter for Wireless Power Transfer Systems", *Eletrônica de Potência*, vol. 30, p. e202542, Jul. 2025, doi:10.18618/REP.e202542.

[18] N. C. D. Pont, D. G. B. Jr, T. B. Lazzarin, I. Barbi, "Conversor CC-CC Paralelo Ressonante Meia Ponte Assimétrico com Saída em Tensão", *Eletrônica de Potência*, vol. 23, no. 1, p. 108–117, Oct. 2017, doi:10.18618/REP.2018.1.2740.

[19] H. Bai, D. Yang, J. Song, Q. Su, B. Duan, C. Zhang, "Linear Active Disturbance Rejection Control of LLC Resonant Converters for EV Chargers", *in 2020 Chinese Automation Congress (CAC)*, pp. 993–998, 2020, doi:10.1109/CAC51589.2020.9327865.

[20] H. Tebianian, Y. Salami, B. Jeyasurya, J. E. Quaicoe, "A 13.56-MHz Full-Bridge Class-D ZVS Inverter With Dynamic Dead-Time Control for Wireless Power Transfer Systems", *IEEE Transactions on Industrial Electronics*, vol. 67, no. 2, pp. 1487–1497, 2020, doi:10.1109/TIE.2018.2890505.

[21] Y. Li, X. Ruan, L. Zhang, Y. K. Lo, "Multipower-Level Hysteresis Control for the Class E DC–DC Converters", *IEEE Transactions on Power Electronics*, vol. 35, no. 5, pp. 5279–5289, May 2020, doi:10.1109/TPEL.2019.2940043.

[22] A. Celentano, F. Pareschi, R. Rovatti, G. Setti, "A Zero-Transient Dual-Frequency Control for Class-E Resonant DC–DC Converters", *IEEE Transactions on Power Electronics*, vol. 38, no. 2, pp. 2105–2114, February 2023, doi:10.1109/TPEL.2022.3208816.

[23] W. Zhu, H. Sekiya, "A 1MHz Class-E2 Single-Stage PFC Converter with Frequency Control", *in 2020 IEEE Applied Power Electronics Conference and Exposition (APEC)*, pp. 2041–2047, 2020, doi:10.1109/APEC39645.2020.9124248.

[24] N. Obinata, W. Luo, X. Wei, H. Sekiya, "Analysis of Load-independent Class-E Inverter at Any Duty Ratio", *in IECON 2019 - 45th Annual Conference of the IEEE Industrial Electronics Society*, vol. 1, pp. 1615–1620, 2019, doi:10.1109/IECON.2019.8927599.

[25] A. Komanaka, W. Zhu, K. Nguyen, H. Sekiya, X. Wei, "Load Independent Class- E1Inverter with Shunt Capacitance", *in 2021 IEEE 30th International Symposium on Industrial Electronics (ISIE)*, pp. 1–6, 2021, doi:10.1109/ISIE45552.2021.9576229.

[26] A. Komanaka, W. Zhu, X. Wei, K. Nguyen, H. Sekiya, "Generalized Analysis of Load-Independent ZCS Parallel-Resonant Inverter", *IEEE Transactions on Industrial Electronics*, vol. 69, no. 1, pp. 347–356, 2022, doi:10.1109/TIE.2021.3053888.

[27] T. Sensui, H. Koizumi, "Load-Independent Class E Zero-Voltage-Switching Parallel Resonant Inverter", *IEEE Transactions on Power Electronics*, vol. 36, no. 11, pp. 12805–12818, 2021, doi:10.1109/TPEL.2021.3077077.

[28] Y. Jiang, J. Liang, H. Wang, Y. Liu, M. Fu, "Load-Impedance-Insensitive Design of High-Efficiency Class EF Inverters", *IEEE Transactions on Power Electronics*, vol. 39, no. 2, pp. 1958–1962, 2024, doi:10.1109/TPEL.2023.3330515.

[29] A. Komanaka, W. Zhu, X. Wei, K. Nguyen, H. Sekiya, "Load-Independent Inverse Class-E ZVS Inverter and its Application to Wireless Power Transfer Systems", *IET Power Electronics*, vol. 15, no. 7, pp. 644–658, 2022, doi:10.1049/PEL2.12256.

[30] W. Luo, X. Wei, H. Sekiya, T. Suetsugu, "Design of Load-Independent Class-E Inverter with MOSFET Parasitic Capacitances", *in 2019 IEEE 62nd International Midwest Symposium on Circuits and Systems (MWSCAS)*, pp. 529–532, 2019, doi:10.1109/MWSCAS.2019.8884834.

[31] C. Cheng, Y. Zhang, X. Zheng, W. Hua, "A Full-Range Soft-Switching Class-E Inverter Achieving Quasi-Constant Voltage Output", *IEEE Transactions on Power Electronics*, vol. 40, no. 6, pp. 7663–7667, 2025, doi:10.1109/TPEL.2025.3541206.

[32] B. Li, K. Ngo, "Analysis and Design of an Isolated Current Source Class-E Inverter With Significant Harmonics", *IEEE Transactions on Power Electronics*, vol. 39, no. 11, pp. 14877–14887, 2024, doi:10.1109/TPEL.2024.3439670.

BIOGRAPHIES

Lucas Sangoi Mendonça is a control and automation engineer (2015), master (2017) and doctor in Electrical Engineering (2021) with the Federal University of Santa Maria. He is currently a professor at Federal University of Technology-Paraná. His areas of interest are: resonant and pwm dc-dc converters, ac-dc resonant rectifiers and dc-ac resonant inverters.

Valmir de Oliveira is an electrical industrial engineer (1993), master (2005) and doctor (2012) in Electrical Engineering and Informatics with the Federal University of Technology-Paraná. His areas of interest are: power electronics, microelectronics and photonics.

Guilherme Stocco Simeão is an undergraduted student in the Mechatronics Engineering Course at Federal University of Technology-Paraná. His areas of interest are: dc-ac inverters and ac-dc rectifiers for wireless power transfer and electric mobility applications.

Fábio Ecke Bisogno is an electrical engineer (1999), master (2001) in Electrical Engineering with the Federal University of Santa Maria, and doctor in Electrical Engineering with the Technische Universität Chemnitz (2006). He is currently a professor at Hochschule Koblenz. His areas of interest are: resonant converters, self-oscillating electronic converters and artificial lighting.